SSRG International Journal of Mechanical Engineering
ISSN: 2348-8360/ https://doi.org/10.14445/23488360/IJME-V11I4P105

Volume 11 Issue 4, 40-55, April 2024
© 2024 Seventh Sense Research Group®

Original Article

The Effects of Heat Treatment on Mechanical Properties and Microstructure of Wire-arc Additive Remanufacturing of AISI 4130 Steel Components

Talent Kachomba[1], James Mutua[2], Joshua Ngoret[2]

[1]*Department of Mechanical and Mechatronic Engineering, Pan African University Institute for Basic Sciences, Technology and Innovation (PAUSTI)-Nairobi, Kenya.*
[2]*Department of Mechanical Engineering, Jomo Kenyatta University of Agriculture and Technology Nairobi, Kenya.*

[1]*Corresponding Author : talentkachomba3@gmail.com*

Received: 06 February 2024 Revised: 24 March 2024 Accepted: 14 April 2024 Published: 30 April 2024

Abstract *- This study focused on the remanufacturing of industrial components using wire-arc additive manufacturing (WAAM) and the influence of heat treatment on the mechanical properties and microstructure evolution of printed parts. The study analyzed the microstructure and mechanical properties in as-built and heat-treated conditions of the 3D printed parts. The results show that the deposited AISI 4130 steel had ferrite-pearlite phases. Microstructural analysis indicated distinct characteristics in the substrate, interface, and deposited regions. Austenitisation and tempering heat treatment caused microstructure homogenization, revealing the predominant ferrite-pearlite phase. The interface had the highest microhardness value of 180.3±6.9 $HV_{0.3}$ in as-built condition. After heat treatment, the hardness improved by an average of 50.2%. The deposited region recorded a density of 7.695 g/cm^3 in an as-built state. In the as-built condition, the test samples exhibited a yield strength of 172.9±2.1 MPa, but the interface sample had 162.1±5.3 MPa. The printed parts had an ultimate tensile stress of ~539.6±68.9 MPa compared to 493.3±21.8 MPa of the substrate. After heat treatment, yield strength improved by 8.9% for the printed part and decreased by 12.1% at the interface region. The ultimate strength for the samples section parallel and perpendicular to the deposition directions increased by 8.0±40.5% and the interface by 36.1%. Fractography analysis indicated that failure changed from brittle to ductile fracture after heat treatment. The findings of this study contribute to designing heat treatment schedules for industrial remanufacturing of structural and functional components using WAAM.*

Keywords *- Wire-arc additive manufacturing, Remanufacturing, Heat treatment, Microstructure, Homogenization.*

1. Introduction

Additive Manufacturing (AM) stands as an innovative digital technology that is revolutionizing the approach to repairing, remanufacturing, and fabricating intricate geometric components. This is achieved by systematically layering materials in successive layers [1, 2]. The common AM technologies that have been employed in the remanufacturing of complex components include cold spray, powder bed fusion [3], Direct Energy Deposition (DED) [4] and laser metal deposition [5]. The DED is a method of AM that forms 3D objects by melting metal material as it is being deposited layer by layer.

This process is facilitated by focused thermal energy. DED offers several significant advantages, including high build speeds, capable of producing dense and strong parts, and excellent metallurgical bonding [6]. The DED technique houses several technologies, such as laser [7], electron beam [8] and Wire-arc Additive Manufacturing (WAAM) [9]. WAAM, like any DED AM technology, is a unique process for constructing large-scale metallic components at remarkably large speeds by using an electric arc as the heat source [10, 11]. The superiority of this technique includes low material consumption, rapid deposition rate, and excellent structural integrity [12].

WAAM provides a critical solution for part remanufacturing [13, 14]. It is exceptional in the manufacturing sector due to its lower production cost when compared to metal powders [15]. WAAM stands as a better candidate for the repair of structural and morphological defects in large-scale metallic components, particularly those used in the mining and aerospace industries [15, 16].

WAAM, a DED technique, enables the manipulation of various deposition parameters. These include welding travel speed, wire feed rate, working distance, arc voltage, current, torch angle, gas flow rate, and the deposition method itself.

This is an open-access article under the CC BY-NC-ND license (http://creativecommons.org/licenses/by-nc-nd/4.0/)

Each of these parameters plays a vital role in influencing the quality of the final product [17, 18]. Ongoing efforts aim to characterize various materials based on their WAAM operating conditions to enhance product quality and facilitate defect repair. However, parameters vary according to the material being used. Critical materials such as the AISI 4130 steel employed in industries for functional and structural complex components often lack comprehensive knowledge regarding repair and remanufacture, resulting in failures [19, 20]. Therefore, the exploration of WAAM in this study is crucial for advancing sustainable and cost-effective manufacturing solutions in these sectors.

The superiority of the final component during repair processes is also affected by the interfacial properties between the substrate and the deposited material [19, 20]. Interface region flaws where the substrate meets the deposited material are prone to arise during repair tasks, potentially resulting in operational failures [21, 22]. Poor quality of WAAM printed parts can be due to a lack of optimized parameters for different materials and an inadequate understanding of the interfacial properties. Previous studies have attempted to optimize the WAAM process parameters and characterize different materials under various operating conditions [23, 24]. However, there is still a gap in the literature regarding the comprehensive understanding of the interfacial properties and the mechanisms leading to defects during the repair process. This study aims to address these gaps and contribute to the improvement of the WAAM process for the manufacturing and repair of critical components in various industrial sectors, such as mining.

Yilmaz et al. [25] proposed a hybrid methodology for repairing aero-engine components. This innovative approach combines reverse engineering, AM, and machining processes. The integration of these techniques allows for a comprehensive and efficient repair process, potentially extending the lifespan of critical aero-engine components. However, the impact of operational conditions on the repaired components was not discussed.

Zhuo et al. [26] noted that tensile fracture of the repaired TC17 interface specimen occurred in the as-deposit zone with numerous dimples. The microstructure analysis showed that martensite was formed in the top zone and changed from superfine lamella α-phase to a banded coarsened lamella α-phase towards the substrate, highlighting the complex microstructure exhibited with the layering process. Onuike et al. [1] considered groove filling as a repair mechanism using AM. The analysis showed a significant increase in hardness by approximately 42% in the heat-treated repaired samples from substrate to deposited layers, highlighting the possible improvements possible with heat treatment.

Heat treatment plays a role in phase formation and transformation [27]. Phase transformation temperatures Ac1 and Ac3 are crucial during heat treatment [28]. These temperatures significantly influence the design of heat treatment processes and the chemical compositions of steel [28]. For austenitisation heat treatment, the temperature has to be 40-50°C above the material's Ac3 value, and the tempering temperature should be below its Ac1 [29]. Heidary et al. [30] carried out heat treatment procedures on AISI 4130 through several procedures. The results underscored the significance of heat treatment in achieving the desired combination of properties. AISI 4130 steel explored in this study finds extensive applications across diverse industries, including aerospace [31], oil and gas [32], mining, and automobile [33, 34]. Its superior heat treatment capabilities enhance toughness, while excellent workability and machinability render it highly versatile in industrial settings [35]. A study by Shim et al. [36] reported an improvement in hardness, yield, and tensile strength of AM-repaired SUS 630 after heat treatment in the substrate, interface, and deposited regions.

The remanufacturing and repair of drilling bits used in the oil, gas, and mining industries present an interesting application potential for WAAM. These drill bits, which are typically manufactured through casting, have complex structures and operate under severe service conditions, making failure inevitable [37, 38] Conventional manufacturing techniques, such as hard die and sand-casting, have been used to produce unique bit configurations, including bi-centre casts. However, these methods are less cost-effective for one-off bit designs and performing repair tasks. The rapid prototyping possible with WAAM can improve the economics of such designs [39].

In addition, WAAM offers significant efficiencies of production and greatly expanded design flexibility, enabling the steel body bits to incorporate improvements on traditional steel body bit configurations as well as performance-enhancing features previously available only in matrix body bit designs [39]. While WAAM has shown promise in various applications, its potential as a repair tool for complex mining drill bits remains largely unexplored in the literature, especially in terms of joint mechanical and microstructural characteristics.

The study focused on assessing the effectiveness of repairing AISI 4130 steel components using the WAAM process. The mechanical properties, microstructure, and fracture surface of the WAAM printed parts in as-built and heat-treated conditions were analyzed and reported. This study sheds light on the feasibility and usefulness of employing the WAAM technique to repair industrial AISI 4130 steel components by exploring mechanical and microstructural properties.

2. Experimental Procedure

2.1. Materials

A 0.9 mm diameter filler Crown Alloy FH-30 4130 wire, provided by Welding Supplies IOC (United States). This filler

wire had mechanical properties of a yield strength of 896 MPa, tensile strength of 1000 MPa, and elongation of 11%. The wire was deposited onto a normalized AISI 4130 alloy steel substrate supplied by Online Metals, USA, which also acted as the control sample. The substrate material data sheets from the manufacturer indicated the following properties: a tensile strength of 670 MPa, yielding at 434 MPa, with 21.50% elongation at the break over a 50 mm length, a density of 7.85g/cm^3 and a Vickers hardness of 177.3 $HV_{0.3}$.

Table 1 shows the chemical composition of the AISI 4130 steel substrate and feedstock wire.

Table 1. AISI 4130 substrate and filler wire chemical composition

Element	C	Mn	Si	Cr	Mo	P	S	Fe
% Wt	0.31	0.5	0.25	0.95	0.2	0.035	0.04	Bal

2.2. Materials

Test parts were prepared using a WAAM custom-made rig in Figure 1. This rig is equipped with an AICO Inverter welder MIG/200 GMAW machine (AICO, Japan). The WAAM setup has a table capable of making movement in the X and Y axes, while the welding torch moves in the Z-axis. This configuration follows the principles of Computer Numerical Control (CNC) mechanisms, providing precise and programmable control over the manufacturing process.

The process parameters employed in the study were previously optimized using the Taguchi design of the experiment. The process parameters were a voltage of 23 V, a current of 120 A, a travel speed of 350 mm/min, and a gas flow rate of 10 L/min of Argo-shield (20% CO_2, 80% Argon). The torch was set at a 90° angle with a height of 12 mm above the substrate, and single bead layers of 70 mm length were deposited during the process. Several layers were deposited for a single bead and following a G-code. After the successful deposition of each layer, a natural air-cooling process was allowed for 30 seconds before commencing the next layer.

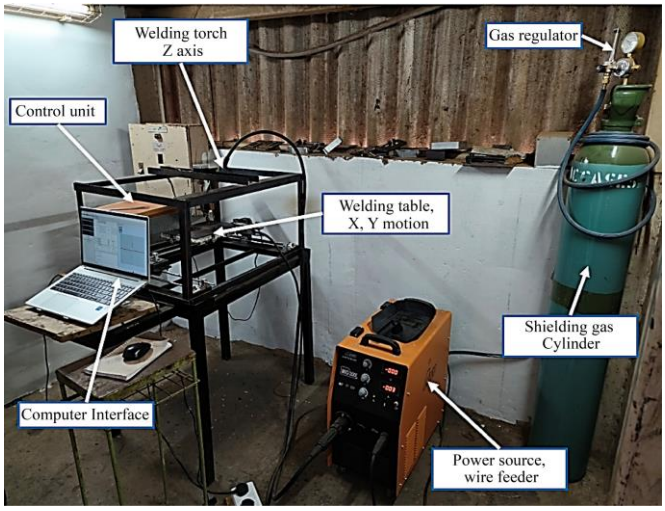

Fig. 1 Experimental WAAM rig setup

2.3. Sample Preparation

Samples for microstructure, microhardness, and tensile analysis were sectioned from the WAAMed components (Figure 2 d)) as indicated in Figure 2 The samples for microstructure and hardness in Figure 2 (a) were extracted using a hand hacksaw with the aid of a coolant. WAAMed samples were then milled to a flat plate on a milling machine. Tensile samples were sectioned out using a Wire Electron Discharge Machine (EDM) as rectangular flat bars. Hand files were used to shape the samples.

2.4. Heat Treatment

The AISI 4130 composition was used to calculate Ac1 and Ac3 temperatures using equations developed by Hougardy equations [40] in Equations (1) and (2). The calculated phase transformation values were: Ac1 (741 °C) and Ac3 (814 °C).

$$Ac1 = 723 - 10.7Mn - 16.9Ni + 29.1Si + 16.9Cr + 6.38W + 290As + 290As \quad (1)$$

$$Ac3 = 910 - 203C0.5 - 15.2Ni + 44.7Si + 104V + 31.5Mo + 13.1W - 30Mn - 11Cr - 20Cu + 700P + 400Al + 120As + 400Ti \quad (2)$$

The austenisation was conducted at 870 °C above its Ac3 temperature for 30 minutes and quenched in water. The tempering process was conducted after the austenisation process at 400 °C below its Ac1 for 1 hour and left to cool at room temperature. These specific conditions were chosen based on the material thickness and the desired balance of mechanical properties. [32, 33]. The heat treatment procedure is summarized in Fig. 3. The heat treatment was conducted using the Muffle furnace (Biobase, China).

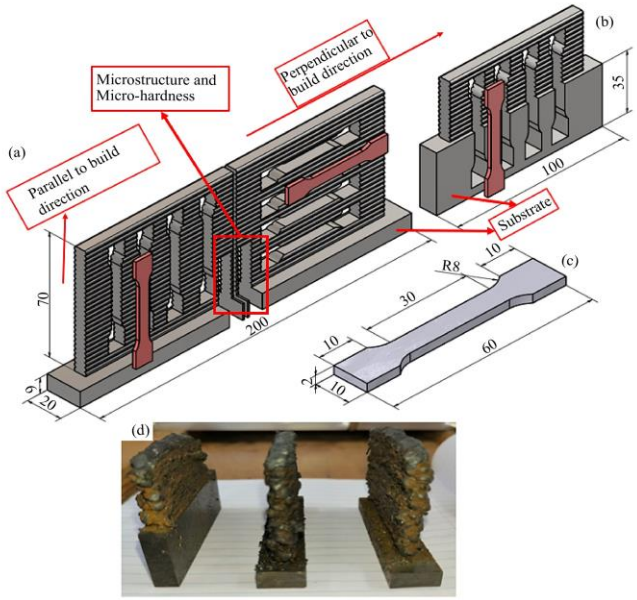

Fig. 2 Tensile samples extraction process (a) Parallel and perpendicular to the build direction, (b) At the interface, (c) Sub-sized tensile sample extraction dimensions in mm, and (d) as-built samples.

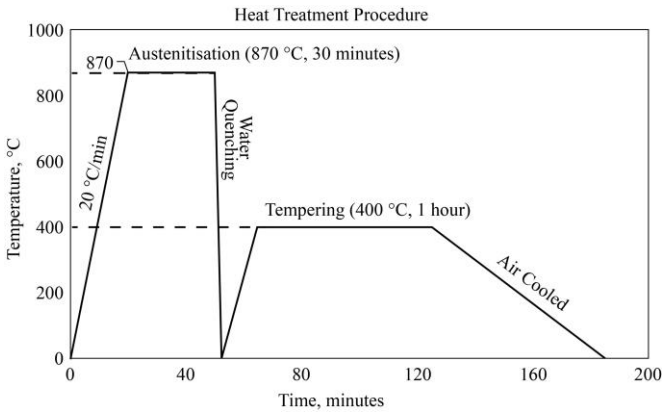

Fig. 3 Heat treatment schedule of AISI 4130 steel in this study

2.5. Microstructure Analysis

The microstructure analysis of the WAAM printed samples was sectioned perpendicular and parallel to the build direction. The sectioned surfaces were polished according to standard metallographic procedures [41]. Grinding was done using 220, 600, and 1200 grit papers, then polished using 3, 1, and 0.25 µm diamond pastes and 1 µm colloidal silica dispersion as per ASTM standard E3-11 [41]. The polished specimens were etched for 10-15 seconds using a 2% Nital solution (2% Nitric acid and 98% ethanol). Microstructural investigation was conducted using the Olympus BX41M-LED Optical Microscope and the JOEL JCM-7000 Benchtop Scanning Electron Microscope (SEM). SEM images were obtained at acceleration voltages of 10kV.

2.6. Microhardness Testing

The Vickers microhardness values of all the 3D printed WAAM samples and the substrate of the AISI 4130 steel were determined. The microhardness was measured on a digital LV800AT Leco Vickers Hardness Tester (Leco Corporation, USA). Microhardness measurements were done by applying 300 gf load and a dwell time of 15 seconds as per ASTM E384-17 [42]. The average microhardness value was determined from three measurements per each section for all the samples tested. The standard deviation for the measured microhardness value was calculated.

2.7. Density Analysis

Density evaluations were performed on various components, including the deposited layers of AISI 4130 in an as-built state, the filler wire, and the substrate sample. Each component underwent three separate density measurements. These measurements were executed using the DahoMeter Electronic Densimeter (DH-300), a product of Guangdong Hongtuo Instrument Technology Co., Ltd., China. This instrument operates based on the Archimedes principle to provide accurate density readings.

2.8. Tensile Testing

Sets of samples in as-built and heat-treated conditions were prepared for tensile testing, as shown earlier in Figure 2 The dimensions of the tensile samples are shown in Figure 2(c). The main consideration for the design and machining of the samples was to maintain 'l/√A' (where 'l' is the gauge length and 'A' is the cross-sectional area of the sample) ratio greater than 4.0 according to ASTM E8 standards [43]. Tensile testing was conducted using an ENKAY Universal testing machine (New Delhi-8, India), with an average loading rate of 200 N/s at room temperature (~ 25°C).

2.9. Fracture Surface Analysis

Post-tensile testing, the broken samples were scrutinized for fracture surface analysis. A JOEL JCM-7000 Benchtop SEM was employed to characterize these fractured surfaces. The images were evaluated in the Secondary Electron Detector (SED) mode, utilizing an acceleration voltage of 15 kV.

3. Results and Discussion

3.1. Microstructure Analysis

Figure 4 shows the initial microstructure of the substrate steel. The microstructure exhibited a lamellar columnar structure composed of ferrite (α) and pearlite ('P').

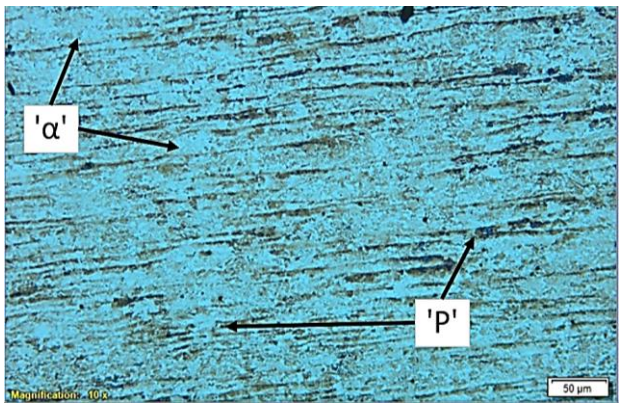

Fig. 4 The initial microstructure of the substrate AISI 4130 steel consisted of large white regions (α-ferrite) and elongated dark regions (Pearlite, 'P')

Fig. 5 shows the microstructure evolution of AISI 4130 in as-built and heat-treated conditions for the substrate region of the sample. The substrate microstructure of AISI 4130 steel in Fig. 5 (a) shows equiaxed ferrite and lamellar pearlite grains. Ferrite is a BCC phase that is relatively soft and ductile, whereas pearlite is a lamellar structure made up of alternating layers of ferrite. The cementite contributes to overall strength and hardness [44].

The austenitisation + quenching in water resulted in a predominant martensite phase because of the rapid cooling. This is well explained with the aid of the Continuous Cooling Transformation (CCT) graph of steels [45]. Upon tempering at 400 °C, the material transitions from martensite, crossing the bainite start boundary and converting the martensite into bainite [33] the slow cooling in the air results in the growth of cementite and ferrite phases. The slow cooling process also

resulted in the formation of ferrite, grain boundaries, and fine and dense lamellar pearlite phases, as shown in Fig. 5 (b).

The material underwent solid solution strengthening as a result of the heat treatment. The heat treatment caused the alloying elements to be absorbed into the iron lattice. This dissolution of elements causes distortion, thus increasing resistance to dislocation movement. As a result of heat treatment, the material's hardness and yield strength improved. Similar findings were reported in the literature [35, 46]. The grain boundaries observed were due to trapped austenite phases, which may have negatively influenced hardness [29, 47].

Fig. 6(a) shows the SEM micrograph of the WAAM-printed AISI 4130 interface region. The microstructure exhibited a network of ferrite and coarse pearlite phases. The presence of a network of ferrite and coarse pearlite phases indicates a complex thermal history experienced by the material. These layers were exposed to excessive heating above and below the material's Ac3. The temperature cycles of the deposition process led to a very slow cooling process of the subsequent layers. These subsequent layers go through the austenite-pearlite transition of the CCT process and, thus, the formation of coarse pearlite [48, 49].

Fig. 6 (b) shows the microstructure of the heat-treated interface region. The microstructure shown exhibits similar characteristics to that of the substrate region in Fig. 5(b). The microstructures of these regions show a high level of homogeneity and a fine ferrite-lamellar pearlite microstructure as a result of the heat treatment.

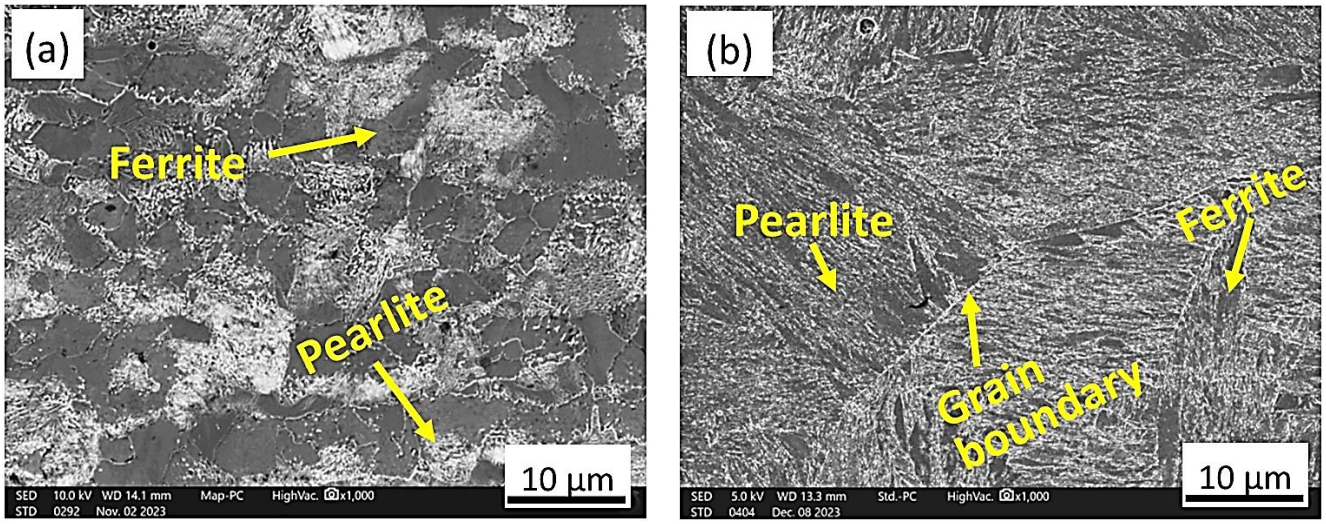

Fig. 5 Microstructure evolution of AISI 4130 substrate in (a) As-built, and (b) Heat treated condition.

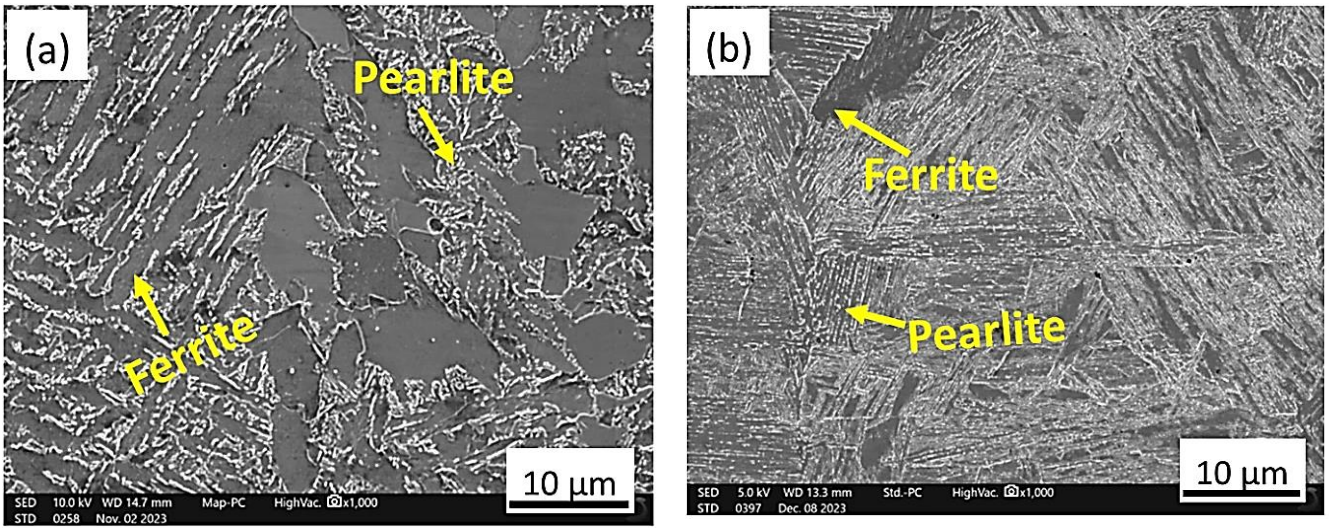

Fig. 6 Microstructure evolution of AISI 4130 interface region in (a) As-built, and (b) Heat-treated condition.

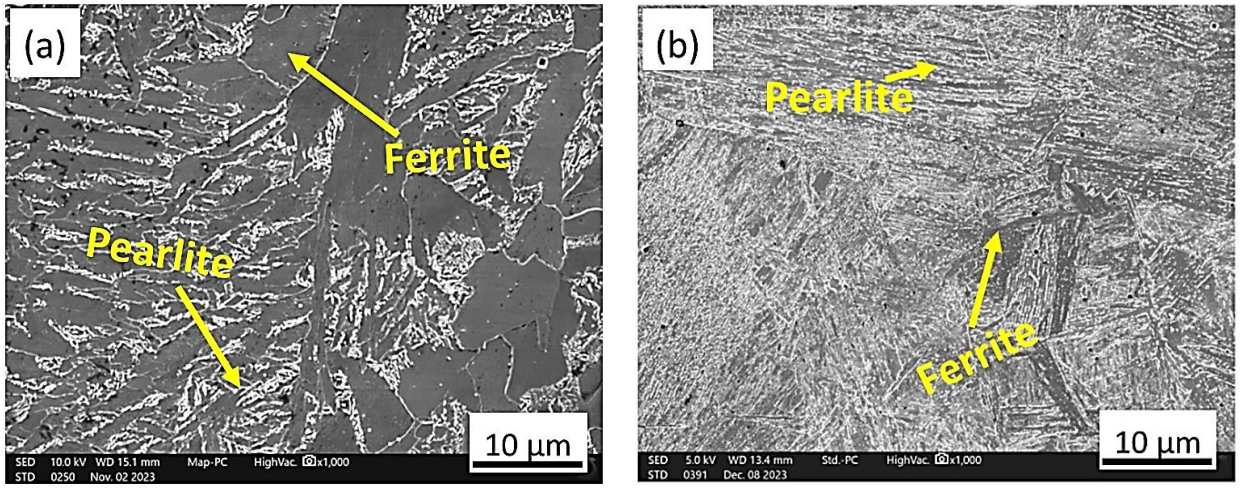

Fig. 7 Microstructure evolution of AISI 4130 deposited region in (a) As-built, and (b) Heat-treated condition.

The microstructural study of the deposited AISI 4130 steel reveals predominant ferrite and coarse pearlite phases, as shown in Figure 7 (a). The existence of these dominant ferrite-pearlite phases is consistent with earlier observations of the interface (Figure 6 (a)) region in the as-built state. The ferrite and pearlite colonies (ferrite and cementite) resulted from the slow cooling process of the deposited regions, causing the austenite-pearlite transition to occur.

The coarse pearlite-ferrite phases, in this instance, are less dense as compared to the interface region. This low relative density of this region indicates that the hardness of the deposited region will likely be lower than that of the interface region in the as-built state. The inter-pass temperature, which is the temperature between the layers, has always been high due to the influence of the new layers being added on top, leading to the slow cooling of the layers [50]. This effect of the inter-pass temperature explains why coarse pearlite and ferrite phases were observed in the deposited region. The slow cooling of steels from the temperature above the material's Ac3 is well reported in the literature with the aid of the CCT diagrams [48, 49].

Upon heat treatment, the microstructure of the deposited (Figure 7 (b)) region undergoes a noticeable transformation towards homogeneity similar to the substrate (Figure 5 (b)) and interface (Figure 6 (b)) regions. The deposited region's heat-treated microstructure exhibited lighter regions in the ferrite-pearlite phases, an indication of lower hardness strength of the deposited regions compared to other heat-treated regions.

The microstructure composition of the as-built regions indicated a coarse ferrite-pearlite structure in the interface and deposited regions. After heat treatment, the microstructure transitioned to a fine homogeneous ferrite-pearlite microstructure. This indicates the positive effect of heat treatment towards microstructure homogenisation and improvement of the hardness as well as the strength of the material.

3.2. Microhardness

Figure 8 shows the microhardness measurements across the substrate, interface and deposited regions of WAAM printed parts. In as-built conditions, uniform hardness distribution was noticed throughout the test sample.

The highest hardness of 180.3±6.9 $HV_{0.3}$ at the interface region can be ascribed to the in-process solid solution strengthening, as reported by Shim et al. [36]. This process involves the dissolution of one phase into another to form a solid solution, which can significantly enhance the material's hardness. The interface region, where the deposited material interacts with the substrate, is subjected to intense thermal cycles during the WAAM process [29]. These thermal cycles may have led to various metallurgical phenomena, such as solid solution strengthening, precipitation hardening, and phase transformations, resulting in increased hardness.

Conversely, the lowest hardness of 150.0±10.2 $HV_{0.3}$ recorded in the substrate region can be explained by the in-process tempering of the substrate, coupled with a very slow cooling process [33]. The cooling rate subsequent to the deposition process may have influenced the hardness of the substrate. A slow cooling process allows for more time for the atoms in the metal to diffuse and form equilibrium microstructures, which are typically softer than the non-equilibrium microstructures formed during rapid cooling. Similar reports are reported in the literature on the effect of slow cooling on the hardness [51, 52]. This may have been resulted in a decrease in hardness.

For the heat-treated condition, the peak hardness of 267.8±16.4 $HV_{0.3}$ was also noted in the interface region. The deposited region exhibited a uniform hardness distribution averaging 232.0±6.6 $HV_{0.3,}$ whilst the substrate region averaged 259.5±0.2 $HV_{0.3}$. The rise in hardness within the substrate, interface and deposited regions by 65.6%, 48.5% and 36.6%, respectively, showcases the effect of controlled heating and cooling towards improved hardness strength. The

improvement in hardness after heat treatment may be a result of solid solution strengthening and grain refinement.

In the as-built condition, the deposited metal's hardness is observed to surpass that of the substrate. This may be due to the thermal cycles experienced during the WAAM process, which can lead to the development of a hardened microstructure in the deposited region [53]. The substrate, manufactured under controlled factory conditions, exhibits a more uniform microstructure, which was then exposed to uncontrolled thermal variations and may have resulted in lower hardness [54].

However, in the heat-treated condition, the hardness of the deposited metal is found to be lower than that of the substrate. This reversal can be explained by the effects of the heat treatment process of the different packing of the two regions manufactured under fully controlled and partially controlled conditions. Meanwhile, the substrate, with its uniform microstructure and packing, responds more predictably and favourably to the heat treatment, maintaining a higher hardness. The less uniform microstructure and packing of the deposited region, resulting from the open-air WAAM process, may also contribute to its less favourable response to heat treatment. The variations in the microstructure could lead to uneven transformations during heat treatment, potentially leading to lower hardness in the deposited regions compared to the substrate regions. When comparing the two conditions, it is clear that heat treatment has a substantial impact on the hardness of the material. However, it is important to note that while increased hardness can improve wear resistance, it can also induce material embrittlement. Therefore, the optimal condition would depend on the specific requirements and application [55].

3.3. Density Analysis

Density measurements of the different components are presented in Table 2. The density measurements of the substrate, wire, and deposited layers provide valuable insights into the material properties and the effects of the WAAM process. The substrate's density represents the initial state of the material before the WAAM process. This density is indicative of the uniform packing and microstructure achieved under controlled factory conditions, as it is in close agreement with the literature [47]. The filler wire had a slightly lower density of 7.811 g/cm³ than the substrate but within range. The slight difference in density between the wire and the substrate could be attributed to variations in manufacturing conditions.

The deposited layers exhibit the lowest density of 7.695 g/cm³. This reduction in density compared to the substrate and wire may be a result of the unique thermal cycles and less controlled packing conditions during the WAAM process. These factors led to the formation of a distinct microstructure in the deposited region, which may have different packing efficiency and, hence, density.

These density measurements, in conjunction with the earlier discussed hardness and microstructure analysis, offer a comprehensive understanding of the material's properties, the effects of the WAAM process and the resultant properties after heat treatment. Within the realm of mining drill bits, the density of the deposited material, as determined by the WAAM process, exhibits a slight deviation of 1.97% lower than the reported density of 7.850 g/cm³ [56] as documented in the literature.

3.4. Tensile Tests

Fig. 9 shows failed tensile test samples of the control substrate and the WAAM printed samples extracted at different orientations. The tensile test results of the substrate plate are shown in Fig. 10. The results indicate that the yield strength decreased by ~ 60% and ultimate tensile strength decreased by ~ 26%, from the manufacturer's specifications stated earlier.

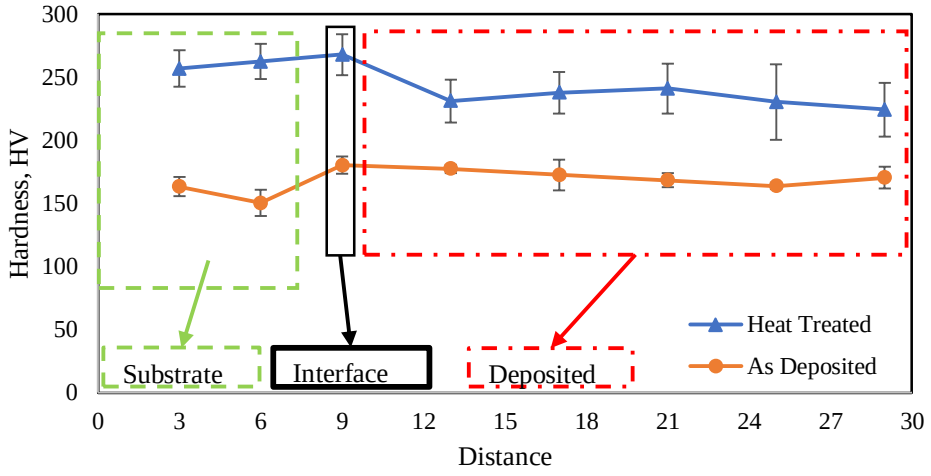

Fig. 8 Summary of hardness test sample and positions of measurement (a) Deposited layers, (b) Interface layer, and (c) Substrate layers.

Table 2. Density measurements of the substrate, wire and deposited region materials

Component	Density, g/cm^3	STDev
Substrate	7.835	0.003
Wire	7.811	0.087
Deposited	7.695	0.016

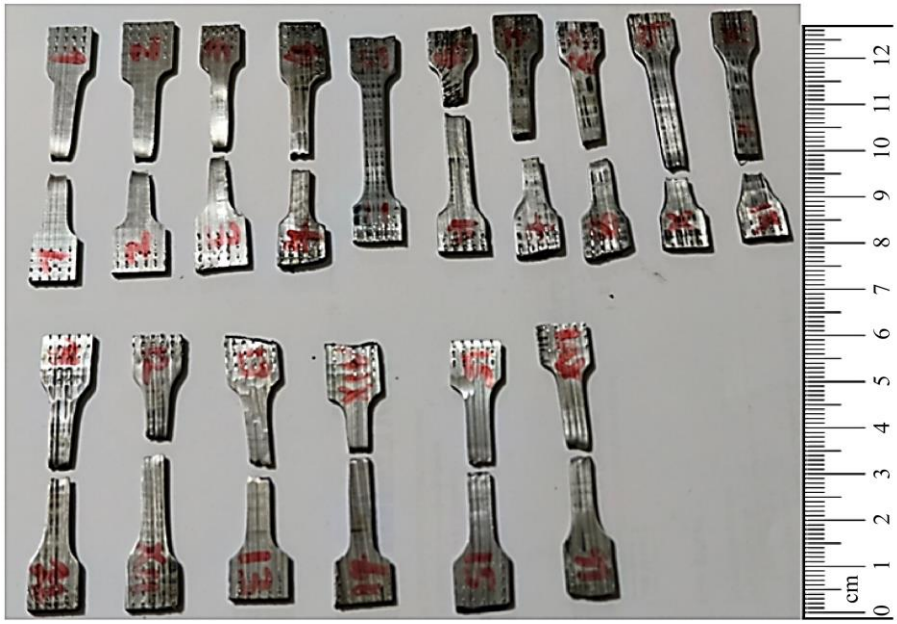

Fig. 9 Strained tensile test samples were extracted from different built orientations

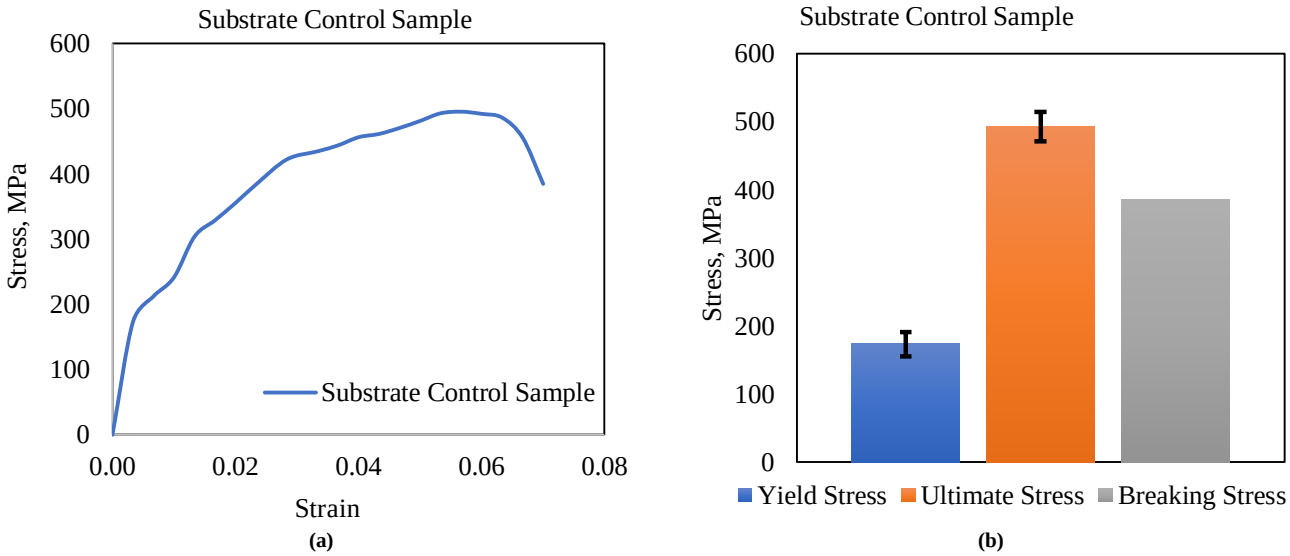

Fig. 10 The plot of tensile test results substrate sample (used as the control sample), (a) Stress-strain graph, and (b) Bar graphs of Yield, Ultimate and Breaking stress.

Fig. 11(a) and (b) show the tensile test results for samples printed parallel to the build direction. The tensile results show similar stress-strain distribution trends compared to the substrate sample (Fig. 10). The yield and ultimate tensile strength for the control substrate sample and for the sample extracted parallel to the build direction in the as-built state fall in the same range (Fig. 11). Heat treatment of the samples deposited parallel to the build direction showed a significant improvement of the yield and ultimate tensile strength by 9.0% and 39.2%, respectively compared to the as-built state. The improved mechanical properties are a result of grain refinement, enhanced interlayer bonding, and precipitation hardening, likely restricting dislocation movement and leading to increased strength [27, 57, 58].

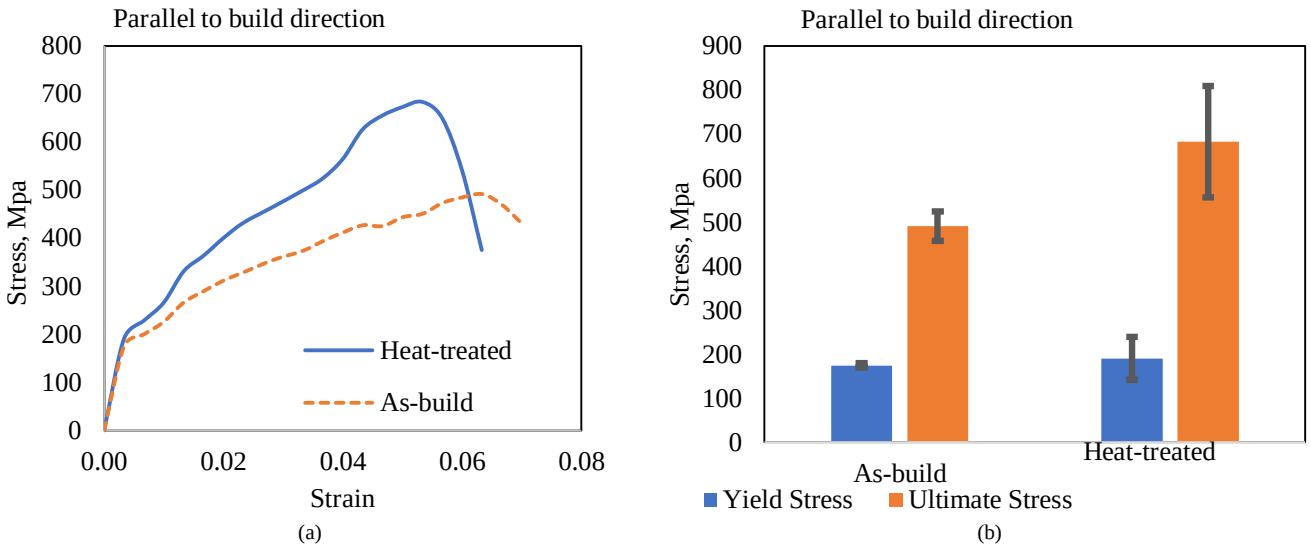

Fig. 11 Plot of tensile properties of samples sectioned parallel to build direction (a) Stress-Strain curve, and (b) Stress vs. yield, and Ultimate stress bar graphs.

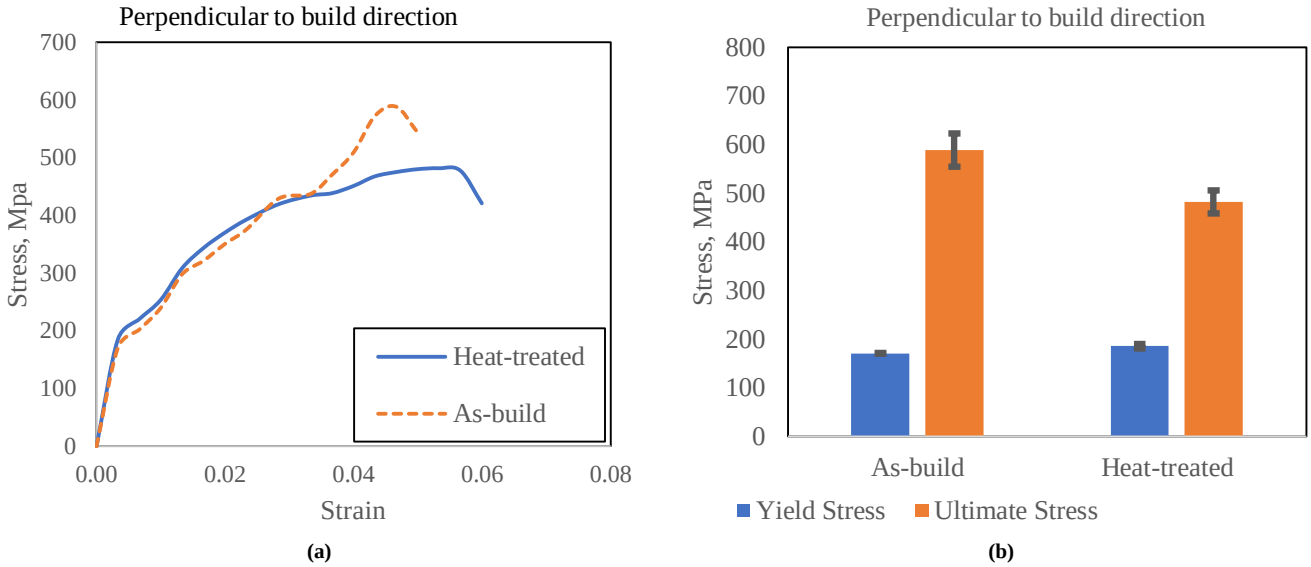

Fig. 12 Plot of tensile properties of samples sectioned perpendicular to build direction (a) Stress-Strain curve, and (b) Stress vs yield, and Ultimate stress bar graphs.

Fig. 12 (a) and (b) show a similar trend to the control substrate sample in yield strength for the as-built samples perpendicular to the build direction. The results show that ultimate tensile strength is larger by 19.3% for samples extracted perpendicular to the build direction compared to the substrate control sample. This is a phenomenon expected as there is minimal influence of interlayer bonding as compared to samples extracted parallel to the build direction.

After heat treatment, there is a great improvement in yield strength and a reduction in ultimate tensile strength by 8.8% and 18.0%, respectively, compared to the as-built state. The samples' ductility and toughness reduced after heat treatment, indicated by their reduction in ultimate tensile strength at low stress, as indicated in Fig. 12(a). This phenomenon has been reported in the literature on the effect of tempering at 400 °C of steels [46] and AISI 4130 [33] being able to increase hardness but may lead to embrittlement, thus reducing tensile strength.

The yield strength for the as-built falls in the normal range as the other samples but with very low ultimate tensile strength for the samples extracted from the interface (deposited region + substrate) (Fig. 13(a) and (b)) region. During the tensile test, the samples failed at the interface region, as shown in Fig. 13 (a). The results indicate that the interface had a weaker region during loading compared to the rest of the samples.

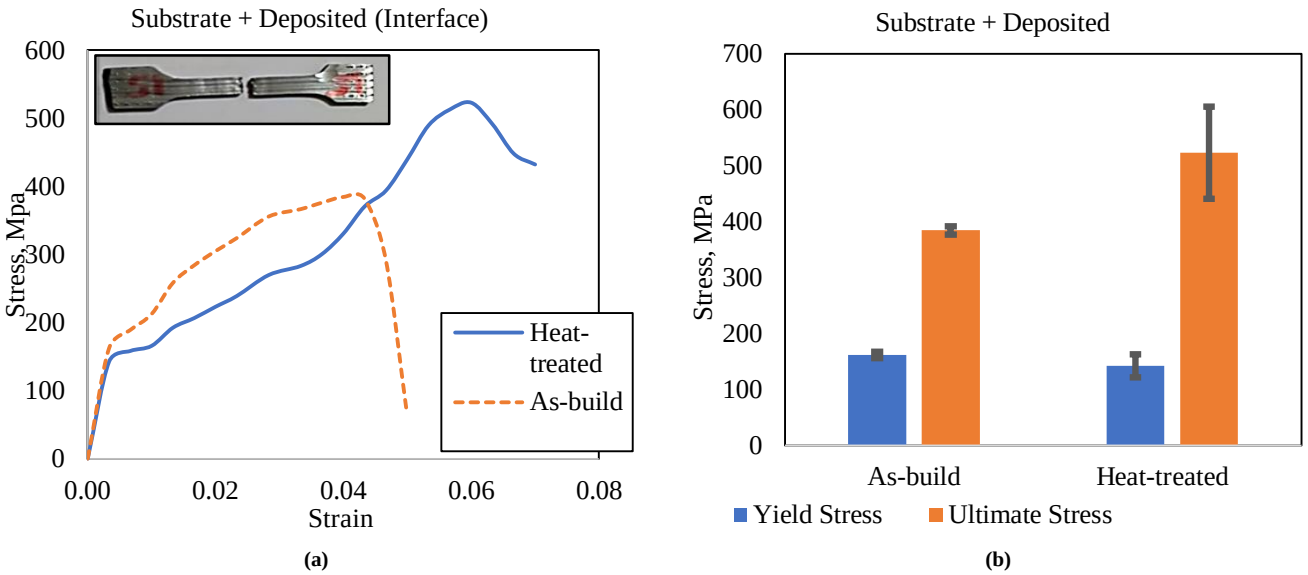

Fig. 13 Plot of tensile properties of samples sectioned at the interface (Substrate + Deposited) (a) Stress-Strain curve, and (b) Stress vs. yield, and ultimate stress bar graphs.

The results show poor interface bonding and brittle nature of the region as a result of low carbon migration, causing deficiency in precipitate formation, hence low solid solution strengthening [59]. Zhuo et al. [26] reported that the interface is more prone to failure due to rapid cooling as the substrate was not preheated and, hence, formed a weak region. Preheating of the substrate has been noted to enhance the bonding strength of the welded AISI 4130 joint [60]. The heat treatment greatly improved the ultimate tensile strength by 36.1% and the elongation as a result of grain refinement and enhanced interface bonding, a phenomenon reported earlier [61].

Generally, the results presented show lower values compared to the standard material properties available in the literature. This may be a result of the thermal cycles experienced during the WAAM processes and the packing of material during the deposition process.

3.5. Fracture Surface Analysis

Fig. 14(a) shows the fracture surface of the substrate control sample. The SEM images reveal considerable slants due to considerable necking of the sample under load. The steep slants indicate a change in cross-sectional area and significant elongation due to the loading as compared to the unstrained sample. The steep slants are a common feature in the ductile fracture of materials [62]. Fig. 14(b) shows a more detailed fracture surface of the tested substrate samples, indicating ductile fracture mode. Fine dimples and tear ridges characterise this region, a result of significant plastic deformation before fracture. These characteristics observed at the fracture surface have been reported to be associated with ductile failure [63].

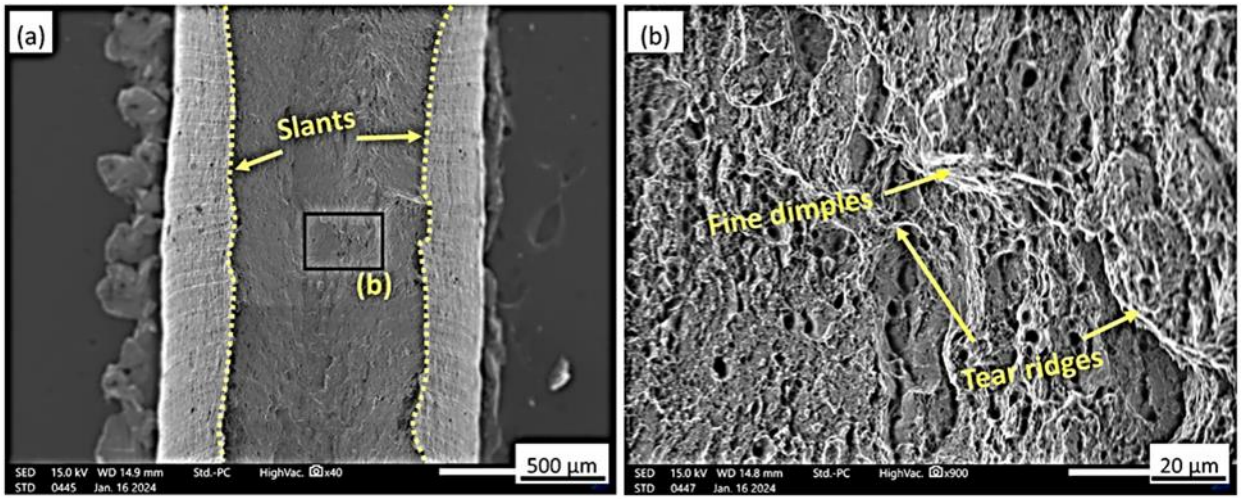

Fig. 14 Fracture surface analysis of AISI 4130 normalised substrate plate subjected to tensile testing

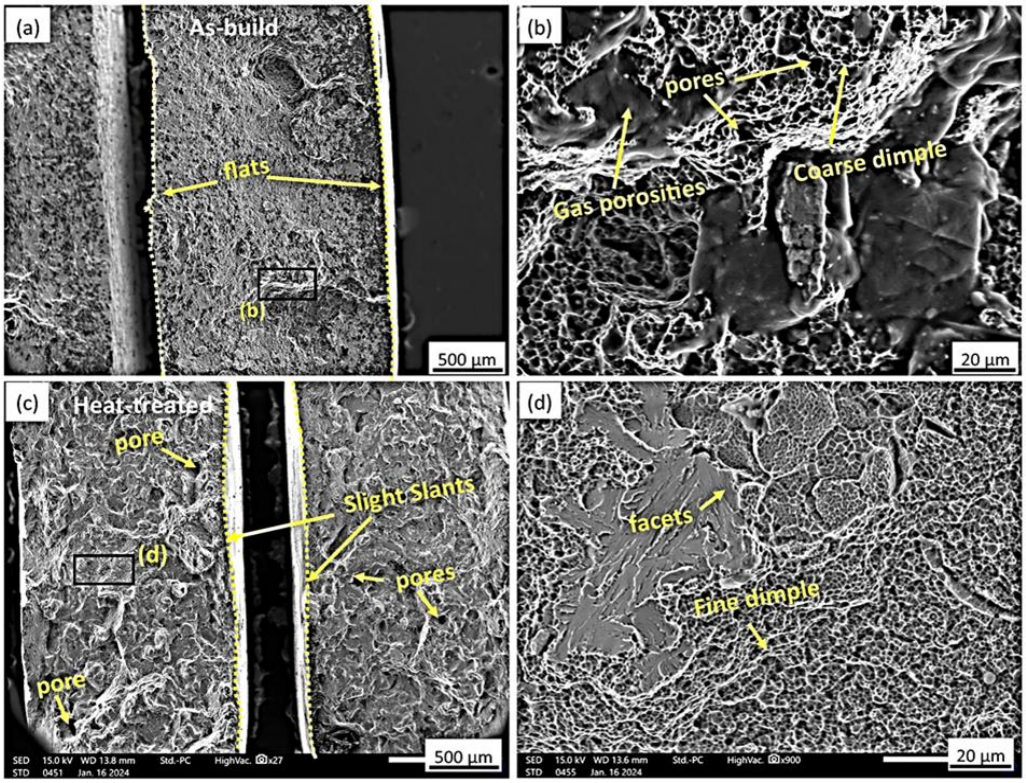

Fig. 15 Fracture surface analysis of AISI 4130 deposited parallel to build direction subjected to tensile testing (a), (b) As-built condition, and (c), (d) Heat-treated condition.

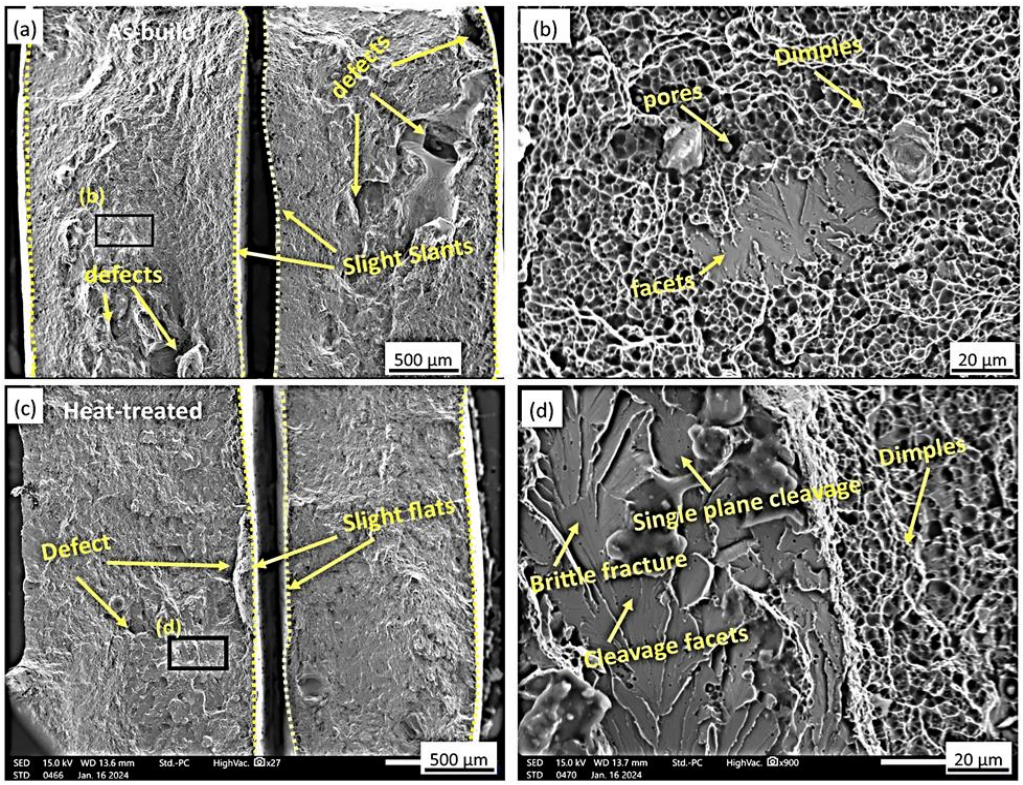

Fig. 16 Fracture surface analysis of AISI 4130 deposited perpendicular to building direction subjected to tensile testing (a), (b) As-built condition, and (c), (d) Heat-treated condition.

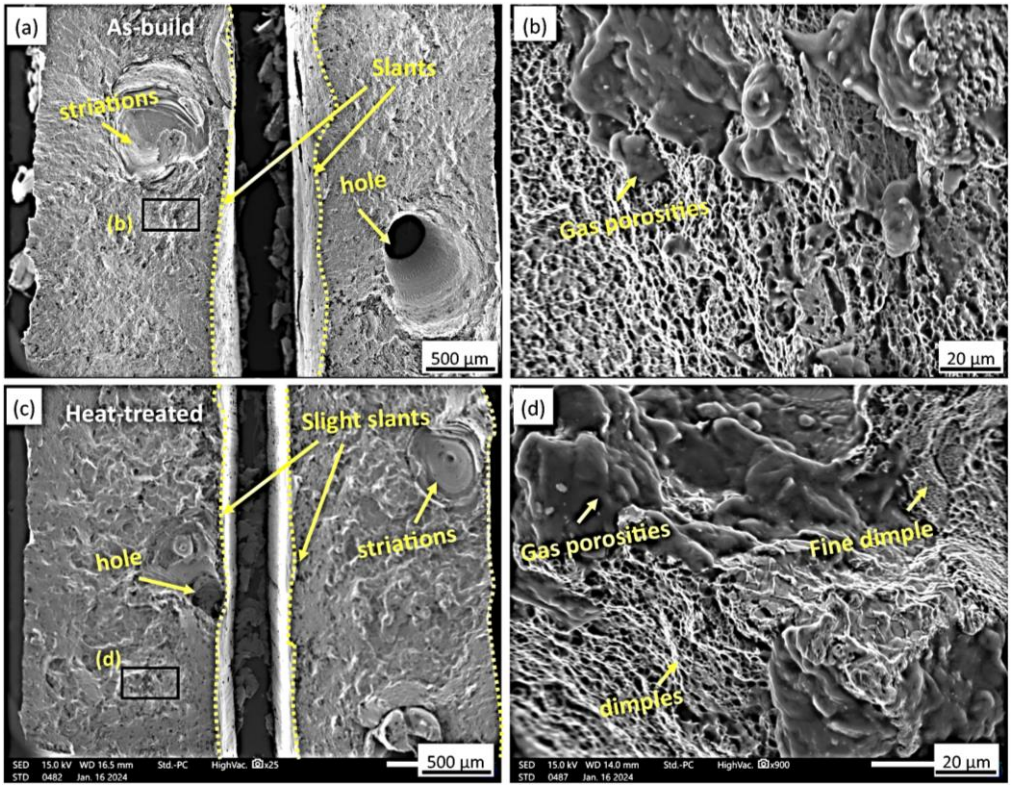

Fig. 17 Fracture surface analysis of AISI 4130 interface (substrate + deposited) region subjected to tensile testing (a), (b) As-built condition, and (c), (d) Heat-treated condition.

In the as-built state, the fracture surface of the sample sectioned parallel to the build direction (Fig. 15(a) and (b)), brittle failure is expected due to the effect of the interlayer bonding. In addition to that, brittle failure occurred as a result of the noticeable defects such as pores, gas porosity, and coarse dimples. Compared to the substrate fracture surface (Fig. 14(a)), where significant cross-sectional area change was observed, cross-sectional area change observed is very low for the fracture surface of samples sectioned parallel to the build direction in (Fig. 15(a)).

The small change in this cross-sectional area is indicated by the flats, which also show minimum necking due to the loading, indicating brittle failure. The gas porosity is also an indication of interlayer fusion leading to the entrapment of gases during the WAAM process. Course dimples are also an indication of brittle fracture [20]. These features suggest imperfections within the material structure and areas where the material has not adequately fused, potentially leading to compromised mechanical properties.

Fig. 15(c) and (d) show the microstructure after heat treatment. The SEM images show features such as facets and fine dimples, suggesting improved ductility and toughness due to grain refinement and enhanced microstructural homogeneity. Pores can still be seen on the fracture surface. Compared to the as-built samples, the change in cross-sectional area is indicated by the presence of slight slanting that occurred due to the loading. This change in the slants shows that the material property has improved from brittleness to ductile and tough nature, as exhibited by the yield and ultimate strength reported earlier in Fig. 11.

Facets seen on the fracture surface indicate areas of significant stress concentration and abrupt fracture propagation. These features suggest that the material experienced rapid and brittle failure [63]. Overall, after heat treatment, the material failed in both ductile and brittle manner. Some regions on the microstructure exhibited the presence of fine dimples. Similar observations have been reported in the literature on the same material [47]. The transition from coarse to fine dimples after heat treatment caused an improvement in tensile properties.

Fig. 16 shows fracture surfaces for samples sectioned perpendicular to the build direction. In the as-built state, Fig. 16 and (b) show the fracture surface, revealing a slight slanting but less pronounced as compared to the substrate sample. Defects in the form of pores are visible across the surface, which may have resulted in early failure. Pores can act as stress concentrators in a material under tensile stress.

The stress concentration occurs because the load applied to the material is not evenly distributed around the pore,

leading to higher stress in the material surrounding the pore [64]. This may have led to the initiation of cracks at the pore sites, which can propagate under continued loading and lead to failure. A single-plane localised facet, the flat and smooth nature of the facet can intensify stress concentration, making the material more susceptible to brittle failure [65]. The facet can act as a plane of weakness where a crack can easily initiate and propagate, leading to failure.

The heat-treated sample (Fig. 16(c) and (d)) had lower microstructural defects than the as-built sample. This is because the high temperatures involved in the heat treatment allow for atoms to diffuse and redistribute more evenly throughout the material. Brittle failure characteristics became more evident, with single-plane cleavage and cleavage facets being dominant post-heat treatment. It was reported in the literature that tempering the AISI 4130 at low temperatures like 400 ℃ leads to improved hardness but also leads to material embrittlement [33].

Figure 17 shows the fracture surfaces of samples extracted at the interface region. The tested samples failed at the interface (Figure 13 (a)) for both as-built and heat-treated conditions. The as-built sample shown in Figure 17 (a) and (b) indicates that the fracture surface exhibited striations where failure might have been initiated. A hole can be seen on the fracture surface approximately 500 µm in diameter. The gas porosities can be observed at the surface an indication of inadequate bonding. The poor bonding has been reported to be eliminated through substrate preheating [60]. The striations, hole, and gas porosities reflect the brittle failure, whilst the slants have some degree of ductile fracture. Heat-treated samples (Figure 17 (c) and (d)), the microstructure exhibited a refined structure with slight slants present and fine dimples, suggesting an improved ductility. In comparison to the as-built, the heat-treated samples showed a more ductile failure which is supported by the tensile properties (Figure 13). Striations and gas porosities can still be seen on the heat-treated fractured surface sample, leading to a reduced yield strength.

4. Conclusion

The samples were prepared using WAAM as a tool for repair and remanufacturing. The mechanical properties and microstructure analysis were evaluated in as-built and heat-treated conditions. The study made the following conclusions:

1. The WAAM-printed AISI 4130 interface initially had a complex microstructure of ferrite and pearlite, leading to maximum hardness in the interface region. Upon heat treatment, the microstructure underwent a noticeable transformation, resulting in a more homogenised ferrite-lamellar pearlite microstructure.
2. The peak hardness for the as-built was observed at the interface (180.3±6.9 $HV_{0.3}$), and the lowest average was recorded in the substrate (150.0 $HV_{0.3}$). Heat treatment led to substantial increases in hardness in the substrate, interface and deposited regions by 65.6%, 48.5% and 36.6%, respectively. The deposited region recorded a density of 7.695 g/cm^3 in an as-built state.
3. In as-built condition, the samples had yield strength of 172.9±2.1 MPa, but the interface sample had 162.1±5.3 MPa. The printed parts had an ultimate tensile stress of ~539.6±68.9 MPa compared to 493.3±21.8 MPa of the substrate. After heat treatment, yield strength improved by 8.9% for the printed part and decreased by 12.1% at the interface region. The ultimate strength for the samples section parallel and perpendicular to the deposition directions increased by 8.0±40.5% and the interface by 36.1%.
4. The fracture surface analysis of the AISI 4130 substrate plate revealed a ductile fracture characterized by fine dimples. However, the fracture surface of the as-built samples indicated the presence of defects and pores, regardless of the sample orientation. The failure mode improved from brittle failure to more ductile fracture in all samples as a result of heat treatment. This suggests that heat treatment can significantly enhance the mechanical properties and performance of WAAM-printed AISI 4130 steel.
5. The findings of this study hold significant implications for stakeholders in the industrial remanufacturing process and underscore the evolving trends in WAAM deposition. By elucidating the relationship between deposition trends and the production of high-quality structural and functional components, this research contributes valuable insights to the field, paving the way for enhanced practices and outcomes in industrial remanufacturing processes.

Acknowledgments

The authors would like to acknowledge and appreciate with gratitude the Pan African University Institute for Basic Sciences, Technology and Innovation (PAUSTI) and the Japan International Cooperation Agency (JICA) for funding this research.

References

[1] Bonny Onuike, and Amit Bandyopadhyay, "Additive Manufacturing in Repair: Influence of Processing Parameters on Properties of Inconel 718," *Materials Letters*, vol. 252, pp. 256-259, 2019. [CrossRef] [Google Scholar] [Publisher Link]

[2] Guijun Bi, and Andres Gasser, "Restoration of Nickel-Base Turbine Blade Knife-Edges with Controlled Laser Aided Additive Manufacturing," *Physics Procedia*, vol. 12, pp. 402-409, 2011. [CrossRef] [Google Scholar] [Publisher Link]

[3] Rahito, D.A. Wahab, and A.H. Azman, "Additive Manufacturing for Repair and Restoration in Remanufacturing: An Overview from Object Design and Systems Perspectives," *Processes*, vol. 7, no. 1, pp. 1-22, 2019. [CrossRef] [Google Scholar] [Publisher Link]

[4] Rahito, Dzuraidah Abd Wahab, and Abdul Hadi Azman, "Restoration of Remanufacturable Components Using Additive Manufacturing," *Proceedings of the 5th International Conference on Sustainable Design and Manufacturing*, vol. 130, pp. 193-198, 2019. [CrossRef] [Google Scholar] [Publisher Link]

[5] H. Koehler et al., "Laser Reconditioning of Crankshafts: From Lab to Application," *Physics Procedia*, vol. 5, pp. 387-397, 2010. [CrossRef] [Google Scholar] [Publisher Link]

[6] Abdollah Saboori et al., "Application of Directed Energy Deposition-Based Additive Manufacturing in Repair," *Applied Sciences*, vol. 9, no. 16, pp. 1-26, 2019. [CrossRef] [Google Scholar] [Publisher Link]

[7] R. Rumman et al., "Laser Metal Deposition and Wire Arc Additive Manufacturing of Materials: An Overview," *Archives of Metallurgy and Materials*, vol. 64, no. 2, pp. 467-473, 2019. [CrossRef] [Google Scholar] [Publisher Link]

[8] David Svetlizky et al., "Directed Energy Deposition (DED) Additive Manufacturing: Physical Characteristics, Defects, Challenges and Applications," *Materials Today*, vol. 49, pp. 271-295, 2021. [CrossRef] [Google Scholar] [Publisher Link]

[9] D.T. Sarathchandra, M.J. Davidson, and Gurusamy Visvanathan, "Parameters Effect on SS304 Beads Deposited by Wire Arc Additive Manufacturing," *Materials and Manufacturing Processes*, vol. 35, no. 7, pp. 852-858, 2020. [CrossRef] [Google Scholar] [Publisher Link]

[10] Laukik P. Raut, and Ravindra V. Taiwade, "Wire Arc Additive Manufacturing: A Comprehensive Review and Research Directions," *Journal of Materials Engineering and Performance*, vol. 30, pp. 4768-4791, 2021. [CrossRef] [Google Scholar] [Publisher Link]

[11] Muralimohan Cheepu, Chang Ik Lee, and Sang Myung Cho, "Microstructural Characteristics of Wire Arc Additive Manufacturing with Inconel 625 by Super-TIG Welding," *Transactions of the Indian Institute of Metals*, vol. 73, pp. 1475-1479, 2020. [CrossRef] [Google Scholar] [Publisher Link]

[12] Reyazul Warsi, Kashif Hasan Kazmi, and Mukesh Chandra, "Mechanical Properties of Wire and Arc Additive Manufactured Component Deposited by a CNC Controlled GMAW," *Materials Today: Proceedings*, vol. 56, pp. 2818-2825, 2022. [CrossRef] [Google Scholar] [Publisher Link]

[13] Tiago A. Rodrigues et al., "Current Status and Perspectives on Wire and Arc Additive Manufacturing (WAAM)," *Materials*, vol. 12, no. 7, pp. 1-41, 2019. [CrossRef] [Google Scholar] [Publisher Link]

[14] C.R. Cunningham et al., "Invited Review Article: Strategies and Processes for High-Quality Wire Arc Additive Manufacturing," *Additive Manufacturing*, vol. 22, pp. 672-686, 2018. [CrossRef] [Google Scholar] [Publisher Link]

[15] Jeong-Hak Lee, Choon-Man Lee, and Dong-Hyeon Kim, "Repair of Damaged Parts Using Wire Arc Additive Manufacturing in Machine Tools," *Journal of Materials Research and Technology*, vol. 16, pp. 13-24, 2022. [CrossRef] [Google Scholar] [Publisher Link]

[16] T.S. Senthil et al., "Mechanical and Microstructural Characterization of Functionally Graded Inconel 825-SS316L Fabricated Using Wire Arc Additive Manufacturing," *Journal of Materials Research and Technology*, vol. 15, pp. 661-669, 2021. [CrossRef] [Google Scholar] [Publisher Link]

[17] Van Thao Le et al., "Wire and Arc Additive Manufacturing of 308L Stainless Steel Components : Optimization of Processing Parameters and Material Properties," *Engineering Science and Technology, an International Journal*, vol. 24, no. 4, pp. 1015-1026, 2021. [CrossRef] [Google Scholar] [Publisher Link]

[18] Yashwant Koli et al., "Investigations and Multi-Response Optimization of Wire Arc Additive Manufacturing Cold Metal Transfer Process Parameters for Fabrication of SS308L Samples," *Journal of Materials Engineering and Performance*, vol. 32, pp. 2463-2475, 2023. [CrossRef] [Google Scholar] [Publisher Link]

[19] Frank Meiners et al., "New Hybrid Manufacturing Routes Combining Forging and Additive Manufacturing to Efficiently Produce High-Performance Components from Ti-6Al-4V," *Procedia Manufacturing*, vol. 47, pp. 261-267, 2020. [CrossRef] [Google Scholar] [Publisher Link]

[20] Anup Kulkarni, D.K. Dwivedi, and M. Vasudevan, "Microstructure and Mechanical Properties of A-TIG Welded AISI 316L SS-Alloy 800 Dissimilar Metal Joint," *Materials Science and Engineering: A*, vol. 790, 2020. [CrossRef] [Google Scholar] [Publisher Link]

[21] Malcolm Dinovitzer et al., "Effect of Wire and Arc Additive Manufacturing (WAAM) Process Parameters on Bead Geometry and Microstructure," *Additive Manufacturing*, vol. 26, pp. 138-146, 2019. [CrossRef] [Google Scholar] [Publisher Link]

[22] Abdulaziz I. Albannai, "A Brief Review on the Common Defects in Wire Arc Additive Manufacturing," *International Journal of Current Science Research and Review*, vol. 5, no. 12, pp. 4556-4576, 2022. [CrossRef] [Google Scholar] [Publisher Link]

[23] Yufeng Xia et al., "Multi-Properties Optimization of Welding Parameters of Wire Arc Additive Manufacture in Dissimilar Joint of Iron-Based Alloy and Nickel-Based Superalloy Using Grey-Based Taguchi Method," *Proceedings of the Institution of Mechanical Engineers, Part C: Journal of Mechanical Engineering Science*, vol. 235, no. 23, pp. 6984-6995, 2021. [CrossRef] [Google Scholar] [Publisher Link]

[24] Fernando Veiga et al., "Wire Arc Additive Manufacturing Process for Topologically Optimized Aeronautical Fixtures," *3D Printing and Additive Manufacturing*, vol. 10, no. 1, pp. 23-33, 2023. [CrossRef] [Google Scholar] [Publisher Link]

[25] Oguzhan Yilmaz, Nabil Gindy, and Jian Gao, "A Repair and Overhaul Methodology for Aeroengine Components," *Robotics and Computer-Integrated Manufacturing*, vol. 26, no. 2, pp. 190-201, 2010. [CrossRef] [Google Scholar] [Publisher Link]

[26] Yimin Zhuo et al., "Microstructure and Mechanical Properties of Wire Arc Additive Repairing Ti–5Al–2Sn–2Zr–4Mo–4Cr Titanium Alloy," *Materials Science and Technology*, vol. 36, no. 15, pp. 1712-1719, 2020. [CrossRef] [Google Scholar] [Publisher Link]

[27] Cui E. Seow et al., "Wire + Arc Additively Manufactured Inconel 718: Effect of Post-Deposition Heat Treatments on Microstructure and Tensile Properties," *Materials & Design*, vol. 183, pp. 1-12, 2019. [CrossRef] [Google Scholar] [Publisher Link]

[28] Wei You et al., "Materialometrical Approach of Predicting the Austenite Formation Temperatures," *Materials Science and Engineering: A*, vol. 419, no. 1-2, pp. 276-282, 2006. [CrossRef] [Google Scholar] [Publisher Link]

[29] Chandan Pandey et al., "Some Studies on P91 Steel and their Weldments," *Journal of Alloys and Compounds*, vol. 743, pp. 332-364, 2018. [CrossRef] [Google Scholar] [Publisher Link]

[30] O. Heidary et al., "UP-Quenched SAE 4130 Steel: Mechanical Properties Assessment and Bainite Formation," *Materials Science and Engineering: A*, vol. 787, 2020. [CrossRef] [Google Scholar] [Publisher Link]

[31] K.M. Rajan, P.U. Deshpande, and K. Narasimhan, "Effect of Heat Treatment of Preform on the Mechanical Properties of Flow Formed AISI 4130 Steel Tubes–A Theoretical and Experimental Assessment," *Journal of Materials Processing Technology*, vol. 125-126, pp. 503-511, 2002. [CrossRef] [Google Scholar] [Publisher Link]

[32] Giuseppe Casalino et al., "Experimental and Numerical Study of AISI 4130 Steel Surface Hardening by Pulsed Nd:YAG Laser," *Materials*, vol. 12, no. 19, pp. 1-19, 2019. [CrossRef] [Google Scholar] [Publisher Link]

[33] O. Heidary et al., "Texture Development during Austempering Process of an AISI 4130 Steel," *Materials Science and Engineering: A*, vol. 793, 2020. [CrossRef] [Google Scholar] [Publisher Link]

[34] Robert P. Mudge, and Nicholas R. Wald, "Laser Engineered Net Shaping Advances Additive Manufacturing and Repair," *Welding Journal-New York*, vol. 86, no. 1, pp. 44-48, 2007. [Google Scholar] [Publisher Link]

[35] Hélène Bultel, and Jean-Bernard Vogt, "Influence of Heat Treatment on Fatigue Behaviour of 4130 AISI Steel," *Procedia Engineering*, vol. 2, no. 1, pp. 917-924, 2010. [CrossRef] [Google Scholar] [Publisher Link]

[36] Do Sik Shim et al., "Effects of Pre- and Post-Repair Heat Treatments on Microstructure and Tensile Behaviors of 630 Stainless Steel Repaired by Metal Additive Manufacturing," *Journal of Materials Research and Technology*, vol. 13, pp. 980-999, 2021. [CrossRef] [Google Scholar] [Publisher Link]

[37] Wei Liu, and Deli Gao, "Hall-Petch Relation in the Fracture Strength of Matrix-Body PDC Bits," *International Journal of Refractory Metals and Hard Materials*, vol. 98, 2021. [CrossRef] [Google Scholar] [Publisher Link]

[38] M.R. Taylor, A.D. Murdock, and S.M. Evans, "High Penetration Rates and Extended Bit Life through Revolutionary Hydraulic and Mechanical Design in PDC Drill Bit Development," *SPE Drilling & Completion*, vol. 14, no. 1, pp. 34-41, 1999. [CrossRef] [Google Scholar] [Publisher Link]

[39] L.M. Smith, V.P. Perrin, and R. Delwiche, "Steel Body PDC Bit Technology Demonstrates Performance Improvements," *IADC/SPE Asia Pacific Drilling Technology*, Jakarta, Indonesia, 1998. [CrossRef] [Google Scholar] [Publisher Link]

[40] Mehran Zamani, Hamed Mirzadeh, and Hamid M. Ghasemi, "Mechanical Properties and Fracture Behavior of Intercritically Annealed AISI 4130 Chromoly Steel," *Materials Research Express*, vol. 5, no. 6, 2018. [CrossRef] [Google Scholar] [Publisher Link]

[41] ASTM E3-11, Standard Guide for Preparation of Metallographic Specimens, American Society for Testing and Materials, pp. 1-12, 2017. [CrossRef] [Publisher Link]

[42] ASTM E384-17, Standard Test Method for Microindentation Hardness of Materials, American Society for Testing and Materials, pp. 1-40, 2022. [CrossRef] [Publisher Link]

[43] ASTM E8/E8M-22, Standard Test Methods for Tension Testing of Metallic, American Society for Testing and Materials, pp. 1-31, 2010. [CrossRef] [Google Scholar] [Publisher Link]

[44] Lioudmila A. Matlakhova et al., "Phase Composition and Temperature Effect on the Dynamic Young's Modulus, Shear Modulus, Internal Friction, and Dilatometric Changes in AISI 4130 Steel," *Crystals*, vol. 13, no. 6, pp. 1-17, 2023. [CrossRef] [Google Scholar] [Publisher Link]

[45] T. Mukherjee et al., "Spatial and Temporal Variation of Hardness of a Printed Steel Part," *Acta Materialia*, vol. 209, 2021. [CrossRef] [Google Scholar] [Publisher Link]

[46] Jiaqing Yin, Mats Hillert, and Annika Borgenstam, "Morphology of Upper and Lower Bainite with 0.7 Mass Pct C," *Metallurgical and Materials Transactions A*, vol. 48, pp. 4006-4024, 2017. [CrossRef] [Google Scholar] [Publisher Link]

[47] M. Abdelwahed et al., "Effect of Water Atomization on Properties of Type 4130 Steel Processed by L-PBF," *Materials & Design*, vol. 210, pp. 1-16, 2021. [CrossRef] [Google Scholar] [Publisher Link]

[48] William D. Callister, and Jr. David G. Rethwisch, *Materials Science and Engineering*, Wiley, 2008. [Google Scholar] [Publisher Link]

[49] R. Steadman, "Materials Science," *Physics Education*, vol. 5, no. 2, 1970. [Google Scholar] [Publisher Link]

[50] P. Wang et al., "Effect of Delta Ferrite on Impact Properties of Low Carbon 13Cr-4Ni Martensitic Stainless Steel," *Materials Science and Engineering: A*, vol. 527, no. 13-14, pp. 3210-3216, 2010. [CrossRef] [Google Scholar] [Publisher Link]

[51] Adnan Çalik, "Effect of Cooling Rate on Hardness and Microstructure of AISI 1020, AISI 1040 and AISI 1060 Steels," *International Journal of Physical Sciences*, vol. 4, no. 9, pp. 514-518, 2009. [Google Scholar] [Publisher Link]

[52] Mengchao Song et al., "Effect of Cooling Rate on Microstructure Evolution and Hardness of Steel Balls," *Transactions of the Indian Institute of Metals*, vol. 73, pp. 913-920, 2020. [CrossRef] [Google Scholar] [Publisher Link]

[53] Markus Köhler, Jonas Hensel, and Klaus Dilger, "Effects of Thermal Cycling on Wire and Arc Additive Manufacturing of Al-5356 Components," *Metals*, vol. 10, no. 7, pp. 1-11, 2020. [CrossRef] [Google Scholar] [Publisher Link]

[54] Fakada Dabalo Gurmesa, and Hirpa Gelgele Lemu, "Literature Review on Thermomechanical Modelling and Analysis of Residual Stress Effects in Wire Arc Additive Manufacturing," *Metals*, vol. 13, no. 3, pp. 1-24, 2023. [CrossRef] [Google Scholar] [Publisher Link]

[55] Witold Brostow, Haley E. Hagg Lobl, and Moshe Narkis, "The Concept of Materials Brittleness and its Applications," *Polymer Bulletin*, vol. 67, pp. 1697-1707, 2011. [CrossRef] [Google Scholar] [Publisher Link]

[56] P.S. Beshenkov et al., "Stress Distribution Analysis of PDC Drill Bits by Computer Modeling," *Eurasian Mining*, no. 2, pp. 25-28, 2017. [CrossRef] [Google Scholar] [Publisher Link]

[57] Teresa Artaza et al., "Wire Arc Additive Manufacturing Ti6Al4V Aeronautical Parts Using Plasma Arc Welding: Analysis of Heat-Treatment Processes in Different Atmospheres," *Journal of Materials Research and Technology*, vol. 9, no. 6, pp. 15454-15466, 2020. [CrossRef] [Google Scholar] [Publisher Link]

[58] Yachao Wang, and Jing Shi, "Effect of Post Heat Treatment on the Microstructure and Tensile Properties of Nano TiC Particulate Reinforced Inconel 718 by Selective Laser Melting," *Journal of Manufacturing Science and Engineering*, vol. 142, no. 5, pp. 1-12, 2020. [CrossRef] [Google Scholar] [Publisher Link]

[59] V. Manivel Muralidaran et al., "Effect of Preheating Temperatures on Impact Properties of Chromoly Alloy Steel 4130 Weld Using Gas Metal Arc Welding," *International Journal of Civil Engineering and Technology*, vol. 8, no. 9, pp. 319-327, 2017. [Google Scholar] [Publisher Link]

[60] Alireza M. Haghighi, and Farhad S. Samani, "Effects of Welding Parameters, Time Interval and Preheating on Residual Stress and Distortion of Joining ST52 Stiffener Ring in an AISI 4130 Tubular Shell," *Acta Mechanica Malaysia*, vol. 3, no. 1. pp. 11-15, 2020. [CrossRef] [Google Scholar] [Publisher Link]

[61] Jian Wang et al., "A Study on Obtaining Equiaxed Prior-β Grains of Wire and Arc Additive Manufactured Ti–6Al–4V," *Materials Science and Engineering: A*, vol. 772, 2020. [CrossRef] [Google Scholar] [Publisher Link]

[62] Shusen Luo, Zesheng You, and Lei Lu, "Thickness Effect on Fracture Behavior of Columnar-Grained Cu with Preferentially Oriented Nanoscale Twins," *Journal of Materials Research*, vol. 32, no. 24, pp. 4554-4562, 2017. [CrossRef] [Google Scholar] [Publisher Link]

[63] Colin Williams et al., "Nondestructive Evaluation of Fracture Toughness in 4130 Steel Using Nonlinear Ultrasonic Testing," *Journal of Nondestructive Evaluation*, vol. 41, 2022. [CrossRef] [Google Scholar] [Publisher Link]

[64] Hanxue Cao et al., "The Stress Concentration Mechanism of Pores Affecting the Tensile Properties in Vacuum Die Casting Metals," *Materials*, vol. 13, no. 13, pp. 1-14, 2020. [CrossRef] [Google Scholar] [Publisher Link]

[65] Chandan Pandey et al., "Homogenization of P91 Weldments Using Varying Normalizing and Tempering Treatment," *Materials Science and Engineering: A*, vol. 710, pp. 86-101, 2018. [CrossRef] [Google Scholar] [Publisher Link]